Towards Synchronous Memorizability and Generalizability with Site-Modulated Diffusion Replay for Cross-Site Continual Segmentation

Dunyuan Xu, Xi Wang, Jingyang Zhang, and Pheng-Ann Heng, *Senior Member, IEEE*

***Abstract*— The ability to learn sequentially from different data sites is crucial for a deep network in solving practical medical image diagnosis problems due to privacy restrictions and storage limitations. However, adapting on incoming site leads to catastrophic forgetting on past sites and decreases generalizablity on unseen sites. Existing Continual Learning (CL) and Domain Generalization (DG) methods have been proposed to solve these two challenges respectively, but none of them can address both simultaneously. Recognizing this limitation, this paper proposes a novel training paradigm, *learning towards Synchronous Memorizability and Generalizability (SMG-Learning)*. To achieve this, we create the orientational gradient alignment to ensure memorizability on previous sites, and arbitrary gradient alignment to enhance generalizability on unseen sites. This approach is named as *Parallel Gradient Alignment (PGA)*. Furthermore, we approximate the PGA as dual meta-objectives using the first-order Taylor expansion to reduce computational cost of aligning gradients. Considering that performing gradient alignments, especially for previous sites, is not feasible due to the privacy constraints, we design a *Site-Modulated Diffusion (SMD)* model to generate images with site-specific learnable prompts, replaying images have similar data distributions as previous sites. We evaluate our method on two medical image segmentation tasks, where data from different sites arrive sequentially. Experimental results show that our method efficiently enhances both memorizability and generalizablity better than other state-of-the-art methods, delivering satisfactory performance across all sites. Our code will be available at: https://github.com/dyxu-cuhkcse/SMG-Learning.**

***Index Terms*— Memorizability, Generalizability, Gradient Alignment, Site-Modulated Diffusion.**

I. Introduction

RECENTLY, Convolutional Neural Network (CNN)-based methods have achieved promising performance in medical image segmentation [1]. Their accuracy relies on a large amount of training data, which is usually gathered from multiple sites (or hospitals) [2], as collecting extensive data from a single site is difficult due to data scarcity [3]. However, strict data sharing policies across sites [4] make it impractical to aggregate these multi-site data into a consolidate set for model training. A privacy-preserving and storage-efficient alternative is to train the model with a data stream, where data of different sites arrives in sequence, while strictly prohibiting the storage and re-accessing of the data from previously learned sites [5].

A straightforward way to utilize this multi-site data stream is consecutively fine-tuning the model solely on the incoming site. However, due to the data heterogeneity exists across sites with varying imaging protocols and scanning devices [2], this model fine-tuning approach would be limited in two aspects: 1) weak memorizability [6], leading to a significant performance drop on previous sites with considerable domain shifts; and 2) limited generalizability, deteriorating the performance on unseen sites with out-of-distribution data [7]. Therefore, it is essential to equip the model with the capability of Learning with Synchronously high Memorizability and Generalizability, referred to as *SMG-Learning*, encouraging a universal performance improvement on both previous and unseen sites during consecutive model training.

However, prevalent researches have recognized that enhancing model memorizability and generalizability as two distinct challenges, each addressed by customized methods, respectively. On one hand, Continual Learning (CL) aims to reduce model forgetting thus enhance the memorizability [8], such as through consolidating memory using regularization terms activated by past knowledge [9], accumulating memory with site-specific expansive networks [10], and replaying data with coordinated optimization particularly for previous sites stored in the replay buffer [11]. These CL approaches establish a unidirectional knowledge transfer from past to current sites [8] that boosts the memorizability highly oriented to previously learned data, but inevitably introducing learning biases and limiting generalization capacity for sites with unseen data distribution. On the other hand, Domain Generalization (DG) is proposed to enable models generalize effectively to unseen sites, with a key aspect of learning invariance [12] against data discrepancy, such as by image-level augmentation to simulate domain shifts [13], and feature-level meta-learning to improve representation invariance [14]. However, despite the efficacy of such invariance learning in achieving generalized performance, these DG methods often lack customized consideration for site-specific knowledge, resulting in unstable performance

D. Xu and X. Wang contributed equally. (Corresponding author: Jingyang Zhang)

D. Xu, X. Wang, J. Zhang and P.-A. Heng are with the Department of Computer Science and Engineering, The Chinese University of Hong Kong, Hong Kong, China. (e-mail: dyxu21, xiwang, pheng@cse.cuhk.edu.hk, zjysjtu1994@gmail.com)

D. Xu, J. Zhang and P.-A. Heng are also with the Institute of Medical Intelligence and XR, The Chinese University of Hong Kong, Hong Kong, China.

X. Wang is also with the Zhejiang Lab, Hangzhou, China.

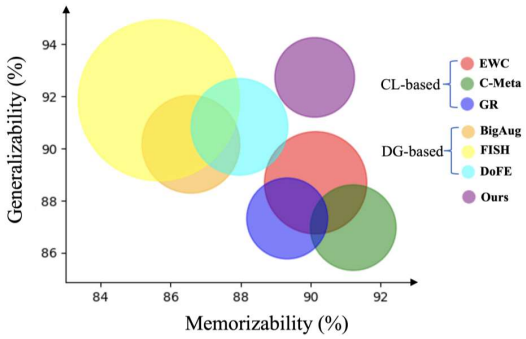

Fig. 1. Comparison between our method with other CL and DG approaches. Memorizability measures the performance on previous sites and generalizability represents the performance on the unseen site. The radius of each distribution reflects the standard deviation across all sites.

balance between current and previous sites and thus weakening memorizability. Overall, existing CL and DG methods can exhibit advantages on either model memorizability or generalizability, yet none of them is capable of SMG-Learning that gains both advantages simultaneously, as illustrated in Fig. 1.

Based on the above problems, the main challenge in SMG-Learning lies in how to build a unified framework that effectively integrates strengths of both CL and DG, given their partial advantages on either memorizability or generalizability. In this work, our insight is to enforce gradients for model updating with *coordination for previous sites* and *invariance across various sites* to achieve this goal. The idea is motivated by the observation that coordinated optimization for previous sites can alleviate historical performance degradation during learning on the current site, as achieved by the gradient similarity for CL [8], while invariant representation across sites promote the performance robustness even for unseen sites, as evidenced by the gradient harmonization for DG [15]. More importantly, these gradient characteristics could be implemented simultaneously following a universal gradient alignment mechanism [16], which consists of two parallel aspects: 1) aligning gradients *orientationally* between previous and current sites to facilitate coordination for strengthened memorizability; and 2) aligning gradients *arbitrarily* within each mini-batch across randomly site-split data subsets to encourage site-invariance for stronger generalizability. Therefore, leveraging this novel perspective of parallel gradient alignment with orientational and arbitrary aspects, holds promise for pursuing SMG-Learning, aiming to synchronize the model memorizability and generalizability in a unified framework.

However, for multi-site data arriving in sequence, achieving such parallel gradient alignment is impractical, since accessing data from previous sites is strictly prohibited [4]. To address the data absence issue, storing raw representative data of these previous sites to construct a replay buffer provides an effective strategy [11], but it is especially infeasible in the medical field due to the privacy leakage risk [17]. Alternatively, generative replay [4] synthesizes data to simulate past site distributions, which has been advanced by diffusion models [18] predominately. Specifically, to replay images scalable for diverse past sites, diffusion models are often guided by predefined prompts, using a Contrastive Language-Image Pretraining (CLIP)-based encoder [19] with hand-crafted text inputs tailored for different sites. These prompts are determined in advance without modification based on site-specific data, potentially misguiding the diffusion model and limiting the replay scalability for diverse sites. Therefore, for the diffusion-based replay, it is desirable to learn adaptable prompts, with each flexibly aligning with a specific site, enabling scalable replay to support the parallel gradient alignment.

In this work, we present a novel framework named SMG-Learning. Specifically, to synchronize the memorizability and generalizability of the model, we provide a unified perspective of leveraging CL and DG strengths by proposing a Parallel Gradient Alignment (PGA) objective with complementary aspects, including an orientational alignment that determines coordinated gradient for previous sites to improve memorizability, and an arbitrary alignment that enforces site-invariance across random split subsets to promote generalizability. However, the direct optimization of the PGA objective in model training is costly as it involves the expensive computational of second-order derivatives. To reduce the computational cost, we propose to approximate the PGA objective as dual meta-objectives using only first-order derivatives for simplification, which is called Dual-Meta optimization. Moreover, as data in previous sites are inaccessible that limits the PGA process, we propose a site-modulated diffusion model for data replay, where adaptable prompts are learned to modulate the diffusion model to generate diverse data distribution scalable for diverse sites. Our main contributions are summarized as follows:

- We propose the Synchronous Memorizability and Generalizability (SMG)-Learning framework for continual cross-site segmentation.
- We present a novel Parallel Gradient Alignment (PGA) algorithm, which alleviates forgetting issue and enhances model generizability through two complementary gradient alignment operations.
- Our Dual-Meta strategy simplifies gradient alignment by using the first-order Taylor expansion to approximate second-order derivatives, reducing computational cost.
- We introduce an effective site-modulated diffusion generative method for creating simulated replay data, guided by site-specific learnable prompts.

A preliminary version of this work was presented in a conference paper [20]. This journal version expands upon the previous include (1) introducing a site-modulated diffusion module for replaying synthesised previous data; (2) providing more comprehensive descriptions of our method; (3) evaluating our method with extensive comparisons to more CL and DG methods; and (4) verifying the effectiveness of our method on extra datasets and performing additional ablation studies.

II. Related Work

A. Continual Learning

Continual Learning (CL)-based methods are designed to alleviate catastrophic forgetting of previous sites when models are sequentially trained on a data stream composed of numerous distinct sites, with domain gap exists between each site due to different protocols and devices. CL-based approaches can be categorized into four groups: 1) Regularization-based

[21] approaches rely on regularized targets such as weight regularization or function regularization; 2) Representation-based [22] approaches exploit the strengths of representations including self-supervised learning, pre-training for downstream, continual pre-training; 3) Optimization-Based [23] approaches aims to design and manipulate the optimization process through methods like gradient projection, meta-learning and loss landscape; 4) Architecture-based [24] methods focusing on task-specific parameter allocation, model decomposition, and modular network. However, these approaches tend to ensure the coordinated gradients for previous and incoming site, which biases the optimization direction and decreases the model generalization capacity [8].

B. Domain Generalization

Domain Generalization (DG)-based methods are designed to maintain model efficiency when generalized to out-of-distribution (OOD) data. These methods utilize strategies such as domain alignment, meta-learning, and ensemble learning to enhance robustness against domain shifts. Specifically, domain alignment focuses on minimizing the discrepancies among the available domains to learn domain-invariant representations [25]. In contrast, meta-learning facilitates future learning by extracting insights from related tasks [26], typically by partitioning the training data into meta-train and meta-test subsets [27]. Lastly, ensemble learning promotes performance by aggregating models trained on different partitions of training data [28]. Despite their effectiveness, DG-based methods often overlook the need to balance performance between previous and incoming sites to maintain accuracy on past data.

C. Replay Buffer Creation

A replay buffer retains a selection of representative raw training samples that are regularly updated [11], and it is utilized in future training to preserve previous learnt knowledge. However, constraints related to privacy and storage efficiency render this approach impractical in clinical situations. To address the privacy restriction, the concept of generative replay has been proposed, which involves training an additional generative model to generate replay data [4]. Recent generative replay methods have employed Generative Adversarial Networks (GANs) [29], Variational Autoencoders (VAEs) [30] and Denoising Diffusion Probabilistic Models (DDPM) [31] as their backbone architectures. Despite their advancements, these models still encounter storage inefficiency issues, as they require preserving generative models for each specific sites. Additionally, these backbones are not scalable to distinct sites, potentially resulting in distorted outputs that is especially significant in the context of medical images.

III. Methodology

Given the constraints of privacy restriction and storage limitation, a model has to consecutively learn from a data stream containing multiple sites, where domain gaps exist between each site. At each training round $t \in [1, T]$, only the incoming site $\mathcal{D}_t = \{\mathcal{X}_t, \mathcal{Y}_t\}$ is available, while previous sites $\{\mathcal{D}_1, ..., \mathcal{D}_{t-1}\}$ and unseen sites $\{\mathcal{D}_{t+1}, ..., \mathcal{D}_T\}$ can not be accessed. With the arrival of $\mathcal{D}_t$, we aim to train a segmentation model ensuring 1) memorizablity, which mitigates catastrophic forgetting on previous sites and 2) generalizability, which adepts to unseen sites efficiently.

Fig. 2 illustrates the main workflow of our proposed SMG-Learning framework. We design the *Parallel Gradient Alignments (PGA)* module contains orientational gradient alignment to enhance memorizability and arbitrary gradient alignment to improve generalizablity. To reduce the computational complexity associated with aligning gradients in PGA, we further approximate the PGA using the first-order Taylor expansion, simplifying it into *Dual Meta* optimization. Additionally, we propose the *Site-Modulated Diffusion (SMD)* utilizing learnable prompts to replay images, constructing the replay buffer to address the issue of inaccessible data from previous sites. The details will be discussed in the following subsections.

A. Parallel Gradient Alignment (PGA)

Updating the model solely with data from incoming site $\mathcal{D}_t$ can lead to overfitting, which causes concurrent performance degradation on previous and unseen sites. To address this issue, an intuitive approach is the naive dual optimization [23], which straightforwardly combines complementary losses try to enhance both memorizability and generalizability. However, these combined losses would be optimized asynchronously due to asymmetrical optimization directions caused by misaligned gradients. Therefore, we propose the Parallel Gradient Alignment (PGA) method to enforce the gradient alignments by utilizing data from $\mathcal{D}_t$ and generated replay buffer $\mathcal{P}$.

1) Naive Dual Optimization: To enhance memorizability, we minimize the combined loss of $L_{\mathcal{D}_t}$ and $L_{\mathcal{P}}$ for maintaining good model performance on incoming and previous sites. To improve generalizability, we integrate $\mathcal{D}_t$ and $\mathcal{P}$ into a unified set $\mathcal{V}$, which is then randomly divided into virtual-train ($\mathcal{V}_{tr}$) and virtual-test ($\mathcal{V}_{te}$) to simulate the domain shift across sites within each mini-batch. Similarly, we minimize the combined loss of $L_{\mathcal{V}_{tr}}$ and $L_{\mathcal{V}_{te}}$ for enhancing the generalizability across sites. The combined losses for naive dual optimization objectives could be formulated as:

$$\begin{aligned} L_{naive}^{\{\mathcal{D}_t,\mathcal{P}\}}(\Theta) &= L_{\mathcal{D}_t}(\Theta) + L_{\mathcal{P}}(\Theta), \\ L_{naive}^{\{\mathcal{V}_{tr},\mathcal{V}_{te}\}}(\Theta) &= L_{\mathcal{V}_{tr}}(\Theta) + L_{\mathcal{V}_{te}}(\Theta). \end{aligned} \tag{1}$$

However, two complementary constraints in each naive dual optimization loss may not be able to achieve simultaneously. For example, $L_{\mathcal{D}_t}(\Theta)$ is easier to be minimized without domain shift in a single site, which dominates the $L_{naive}^{\{\mathcal{D}_t,\mathcal{P}\}}(\Theta)$, yet potentially increase risk of $L_{\mathcal{P}}(\Theta)$ due to the misalignment of optimization directions. In this instance, the model sacrifices its performance on previous sites to fit on the incoming site. Similarly, it is not able to perform simultaneous optimization with $L_{naive}^{\{\mathcal{V}_{tr},\mathcal{V}_{te}\}}(\Theta)$ on random-split subset pairs ($\mathcal{V}_{tr}$, $\mathcal{V}_{te}$) due to the inconsistent gradients, which hinders the ability to extract site-invariant features for generalizing to unseen sites.

2) PGA Objective: To address the issue in naive dual optimization, we propose the *Parallel Gradient Alignment (PGA)* module that synchronously decreases $L_{\mathcal{D}_t}(\Theta)$ and $L_{\mathcal{P}}(\Theta)$ to mitigate forgetting using orientational gradient alignment, and concurrently optimize the model on $\mathcal{V}_{tr}$ and $\mathcal{V}_{te}$ to facilitate

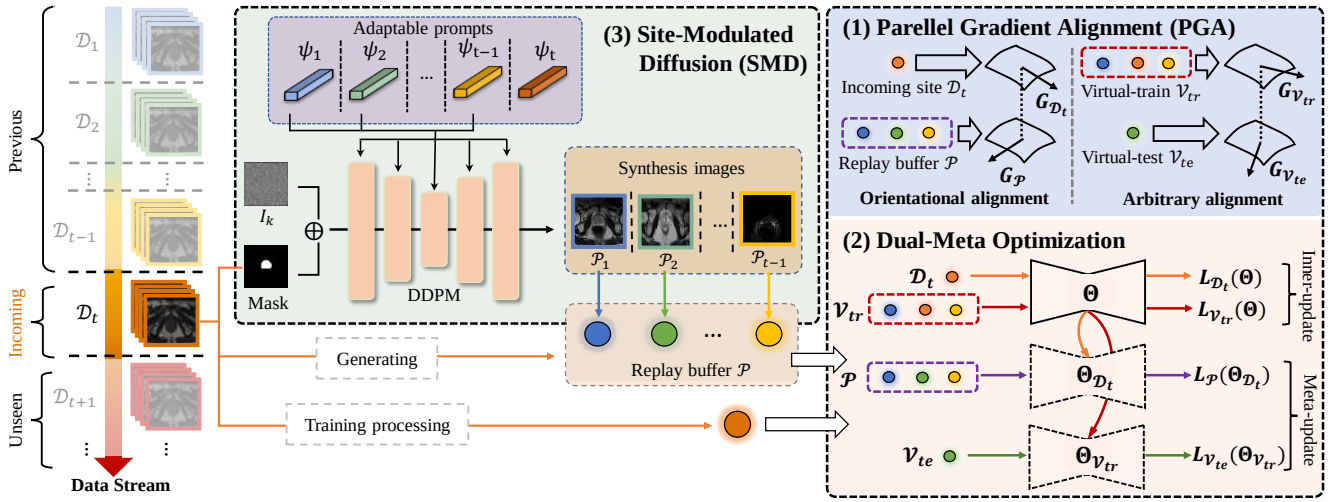

Fig. 2. Overview of the training procedure of our SMG-Learning framework. Upon the arrival of site $\mathcal{D}_t$, we train the segmentation model using *Parallel Gradient Alignment (PGA)* to improve model memorizability and generalizability, as illustrated in part (1). To further reduce the computational cost in aligning gradients, we approximate the PGA with the *Dual-Meta* optimization, as presented in part (2). We design the *Site-Modulated Diffusion (SMD)* module for creating replay buffer to address the data absence issue in previous sites, as shown in part (3).

the generalizability with arbitrary gradient alignment. Let us consider the gradients of losses on $\mathcal{D}_t$, $\mathcal{P}$, $\mathcal{V}_{tr}$, and $\mathcal{V}_{te}$:

$$G_{\mathcal{D}_t} = \frac{\partial L_{\mathcal{D}_t}(\Theta)}{\partial \Theta}, G_{\mathcal{P}} = \frac{\partial L_{\mathcal{P}}(\Theta)}{\partial \Theta}, \\ G_{\mathcal{V}_{tr}} = \frac{\partial L_{\mathcal{V}_{tr}}(\Theta)}{\partial \Theta}, G_{\mathcal{V}_{te}} = \frac{\partial L_{\mathcal{V}_{te}}(\Theta)}{\partial \Theta}. \tag{2}$$

Assuming that $G_{\mathcal{D}_t}$ and $G_{\mathcal{P}}$ have similar direction, forming an acute angle denoted by the condition that the inner product $G_{\mathcal{D}_t} \cdot G_{\mathcal{P}} > 0$ [14], model enhancement along with either $G_{\mathcal{D}_t}$ or $G_{\mathcal{P}}$ will yield an improvement on both $\mathcal{D}_t$ and $\mathcal{P}$. It can also be inferred that, if the directions of $G_{\mathcal{V}_{tr}}$ and $G_{\mathcal{V}_{te}}$ are similar, as indicated by $G_{\mathcal{V}_{tr}} \cdot G_{\mathcal{V}_{te}} > 0$ [14], the extracted features are anticipated to be site-invariant, irrespective of the optimization direction nor the random data partitioning into $\mathcal{V}_{tr}$ and $\mathcal{V}_{te}$, thus potentially augmenting the model generalizablity.

Based on this perspective, we propose to update model with parallel maximization of both $G_{\mathcal{D}_t} \cdot G_{\mathcal{P}}$ and $G_{\mathcal{V}_{tr}} \cdot G_{\mathcal{V}_{te}}$, which is designed to attain synchronous memorizability and generalizablity. Orientational gradient alignment between the incoming site and the replay buffer is achieved by maximizing $G_{\mathcal{D}_t} \cdot G_{\mathcal{P}}$, enforcing the coordinated model optimization on incoming site and previous sites. Concurrently, maximization of $G_{\mathcal{V}_{tr}} \cdot G_{\mathcal{V}_{te}}$ facilitates arbitrary gradient alignment across randomly split subsets, promoting the invariance of extracted features across different sites. Our novel approach PGA is formularized by subtracting $G_{\mathcal{D}_t} \cdot G_{\mathcal{P}}$ and $G_{\mathcal{V}_{tr}} \cdot G_{\mathcal{V}_{te}}$ from the previous naive dual optimization objectives with learning rate γ and β respectively:

$$\begin{aligned} L_{\mathrm{PGA}}(\Theta) =& L_{\mathcal{D}_t}(\Theta) + L_{\mathcal{P}}(\Theta) - \gamma G_{\mathcal{D}_t} \cdot G_{\mathcal{P}} \\ &+ L_{\mathcal{V}_{tr}}(\Theta) + L_{\mathcal{V}_{te}}(\Theta) - \beta G_{\mathcal{V}_{tr}} \cdot G_{\mathcal{V}_{te}}. \end{aligned} \tag{3}$$

3) Compare with CL and DG: The orientational alignment in $L_{\mathrm{PGA}}(\Theta)$ can be regarded as an improvement to the CL paradigm, as we explicitly define the synchronous gradient descent to achieve coordinated optimization without inequality constraints compared with [32]. Simultaneously, the arbitrary alignment draws inspiration from the fundamental concept of DG, which employs random data splitting to simulate domain shift in each mini-batch for invariant feature extraction. Our PGA objective integrates the complementary strengths from these strategies in a unified manner to achieve learning towards synchronous memorizability and generalizabiltiy, delivering promising segmentation performance across all sites.

B. Dual-Meta Optimization

The proposed PGA strategy is powerful yet time-consuming since it aims to minimize the loss of the gradient inner products, which requires the calculation of second-order derivatives. To reduce its computational cost, we propose to approximate the PGA objective using first-order Tylor expansion and optimize it as dual meta-objectives named Dual-Meta.

1) Dual-Meta Algorithm: Considering the expensive time cost for aligning gradients, we efficiently optimize the PGA by approximating it as dual meta-objectives using the first-order Taylor expansion with infinitesimal omitted:

$$\begin{aligned} L_{\mathrm{PGA}}(\Theta) = & \underbrace{L_{\mathcal{D}_t}(\Theta) + L_{\mathcal{P}}\left(\Theta - \gamma G_{\mathcal{D}_t}\right)}_{\text{the first meta-objective}} + \\ & \underbrace{L_{\mathcal{V}_{tr}}(\Theta) + L_{\mathcal{V}_{te}}\left(\Theta - \beta G_{\mathcal{V}_{tr}}\right)}_{\text{the second meta-objective}}, \end{aligned} \tag{4}$$

where $L_{\mathcal{P}}\left(\Theta - \gamma G_{\mathcal{D}_t}\right) = L_{\mathcal{P}}(\Theta) - \gamma G_{\mathcal{P}} \cdot G_{\mathcal{D}_t}$ and $L_{\mathcal{V}_{te}}\left(\Theta - \beta G_{\mathcal{V}_{tr}}\right) = L_{\mathcal{V}_{te}}(\Theta) - \beta G_{\mathcal{V}_{te}} \cdot G_{\mathcal{V}_{tr}}$.

In this formula, each meta-objective is responsible for a distinct alignment operation: the first ensures the orientational gradient alignment between the incoming and past sites (i.e., maximizing $G_{\mathcal{D}_t} \cdot G_{\mathcal{P}}$), for promoting the memorizability. The second meta-objective guarantees the arbitrary gradient alignment between randomly site-split subsets (i.e., maximizing $G_{\mathcal{V}_{tr}} \cdot G_{\mathcal{V}_{te}}$), for generalizing to unseen sites efficiently.

2) Meta-Optimization: As demonstrated in Eq. (4), we refine our PGA algirthm into dual meta-objectives (we name it *Dual-Meta*), the reformulated L_{PGA} can be simplified as:

$$L_{\mathrm{PGA}} = L_{\mathcal{D}_t}(\Theta) + L_{\mathcal{P}}\left(\Theta_{\mathcal{D}_t}\right) + L_{\mathcal{V}_{tr}}(\Theta) + L_{\mathcal{V}_{te}}\left(\Theta_{\mathcal{V}_{tr}}\right), \tag{5}$$

where $\Theta_{\mathcal{D}_t} = \Theta - \gamma G_{\mathcal{D}_t}$ and $\Theta_{\mathcal{V}_{tr}} = \Theta - \beta G_{\mathcal{V}_{tr}}$.

Updated L_{PGA} can be divided into two stages: (1) the inner-update, where the parameters Θ are fine-tuning on $\mathcal{D}_t$ and $\mathcal{V}_{tr}$

with learning rate γ and β respectively, (2) the meta-update, $L_{\mathcal{P}}$ and $L_{\mathcal{V}_{te}}$ are calculated on $\mathcal{P}$ and $\mathcal{V}_{te}$ based on the updated parameters $\Theta_{\mathcal{D}_t}$ and $\Theta_{\mathcal{V}_{tr}}$, but optimized towards the original parameters Θ, as shown in Eq. (5). This approach optimizes the initialization parameters for better adapting on unseen sites with only the first-order derivative calculations are required.

C. Site-Modulated Diffusion (SMD) for Replay

There still exists a significant challenge in the implementation of PGA, which is the reconstruction of the replay buffer for previous sites without re-accessing the raw data. Existing replay buffer creation methods are primarily based on generative methods, which has been dominated by diffusion models [18] with site-specific fixed prompts for guiding the diffusion process. However, these predefined prompts have limited scalability and inefficient adaptability to diverse sites. Therefore, we propose a novel Site-Modulated Diffusion (SMD) method, which employs learnable prompts to modulate the diffusion model for adapting to different sites, creating a replay buffer that simulates the data distributions of previous sites.

1) Traditional Diffusion Process: Traditional diffusion model involves a forward process for adding noise to create a series of noisy images and a backward process for denoising to simulate original images. During the forward process, noise is incrementally accumulated on the original image $\mathcal{I}_0$ over the timestep $k \in [0, K]$, which can be represented as:

$$\mathcal{I}_k := \sqrt{\bar{\alpha}_k}\mathcal{I}_0 + \sqrt{1-\bar{\alpha}_k}\epsilon, \tag{6}$$

where α_k represents the noise level and noise $\epsilon \sim \mathcal{N}(0, \mathbf{I})$.

Given the noisy image as input, the denoising network ϵ_θ is trained to recover the original image with the loss function:

$$\mathcal{L} = \mathbb{E}_{\mathcal{I}_0,k,\epsilon\sim\mathcal{N}(0,\mathbf{I})}\left[\|\epsilon - \epsilon_\theta\left(\mathcal{I}_k, k\right)\|_2^2\right]. \tag{7}$$

To better synthesis images with precise segmentation masks, an intuitive way is to train the diffusion model using channel-wisely concatenated image-mask pairs, where the masks $\mathcal{Y}_t$ come from the incoming site $\mathcal{D}_t$. During the forward process, noise will accumulate only on the image channels for training the denoising network ϵ_θ. Furthermore, to guide the diffusion process, the fixed prompts extracted from different site-specific text captions will also be included. In conclusion, for each mask $\mathcal{Y}_t^i \in \{\mathcal{Y}_t^1, ..., \mathcal{Y}_t^n\}$ from $\mathcal{D}_t$, diffusion model generates replay data using fixed prompt ψ_i extracted from $\mathcal{D}_i$ to create a replayed dataset $\mathcal{P}_i = \{x_i^1, ..., x_i^n\}$ without accessing the raw data, which exhibits similar data distribution as previous site $\mathcal{D}_i$. The loss function in Eq. (7) can be modified into:

$$\begin{aligned}\mathcal{L} = \mathbb{E}_{\mathcal{I}_0,\mathcal{Y}_t,k,\psi_i,\epsilon\sim\mathcal{N}(0,\mathbf{I})}\left[\|\epsilon - \epsilon_\theta\left(\mathcal{I}_k \oplus \mathcal{Y}_t, k, \psi_i\right)\|_2^2\right], \\ \psi_i = F_{frozen}\left(\mathrm{T}_i\right),\end{aligned} \tag{8}$$

where T_i means the text caption for site $\mathcal{D}_i$, F_{frozen} represents the frozen prompt extractor to generate fixed prompt ψ_i from T_i, and $\oplus$ represents the channel-wise concatenation.

As shown in Eq. (8), most traditional diffusion approaches incorporate a frozen Natural Language Processing (NLP)-based prompt extractor, such as CLIP, to extract site-specific fixed prompts from texture captions, thereby guiding the diffusion process. However, such inflexible prompt extractor is not effective at generating the prompts in the medical field due to the domain gap between nature language and clinical terminology, resulting in unsatisfactory guidance during diffusion process. Furthermore, the fixed prompts have limited replay scalability for diverse sites and potentially misguide the diffusion model when more sites are incorporated for training.

2) Site-Modulate Diffusion with Learnable Prompts: In order to solve the problem raised by the frozen NLP-based prompt extractors and inflexible prompts, we propose to control the diffusion process using learnable site-specific prompts, whose scalability enhances the generation results to be more precise across sites. These site-specific learnable prompts are trained and preserved independently for each previous site, and are used to replay previous images before segmentation model is adapted to a new incoming site. We can include the derivation of learnable prompts into diffusion training process as:

$$\psi_i = \underset{\psi_i}{\operatorname{argmin}}\|\epsilon - \epsilon_\theta\left(\mathcal{I}_k \oplus \mathcal{Y}_t, k, \psi_i\right)\|^2. \tag{9}$$

The diffusion learning framework is also modified with the introduction of learnable prompts. Specifically, with the arrival of $\mathcal{D}_t$, we construct the replay buffer $\mathcal{P} = \{\mathcal{P}_1, \mathcal{P}_2, ..., \mathcal{P}_{t-1}\}$ with all $t-1$ preserved learnable prompts, replaying images for previous $t-1$ sites. The diffusion model will then be updated together with t learnable prompts (include one newly added prompt for $\mathcal{D}_t$) on replay buffer and incoming site. This strategy efficiently improves the scalability of the diffusion model for replaying images without re-accessing the raw data.

IV. Experiments

A. Datasets and Experiment Settings

1) Prostate Image Segmentation: We used well-established multi-site MRI data for prostate segmentation [33] collected from six different data sources: RUNMC [34] (Site A), BMC [34] (Site B), HCRUDB [35] (Site C), UCL [36] (Site D), BIDMC [36] (Site E) and HK [36] (Site F). They are collected under different in/through plane resolution between 0.25/2.2-3 and 0.625/3.6 mm. For pre-processing, each image was resized to 256×256 in axial plane and normalized between $[-1, 1]$. In each site, we randomly selected 60%, 15% and 25% of cases for training, validation and testing.

2) Cardiac Image Segmentation: We further utilized a publicly available Cardiac Magnetic Resonance (CMR) segmentation dataset obtained with four vendors collected using distinct devices [37]: Vendor A with Siemens, Vendor B with Philips, Vendor C with GE; and Vendor D with Cannon. All samples are collected under different in-plane resolution ranging from 0.85 to 1.45 mm. We pre-processed each sample into a unit spacing and center-cropped them around the cardiovascular region. Each image was resized to 256×256 in axial plane and normalized to $[-1, 1]$. Each sample contains three distinct foreground labels: the left ventricle (LV), the right ventricle (RV), and the left ventricular myocardium (MYO). For each site, the samples were randomly divided into a training set (50%), a validation set (25%), and a testing set (25%).

3) Experiment Setting and Evaluation Metrics: We arranged the sites to arrive in an alphabetical order, A→B→C→D→E for prostate dataset with unseen site F, A→B→C for cardiac dataset with unseen site Vendor D. The unseen sites were

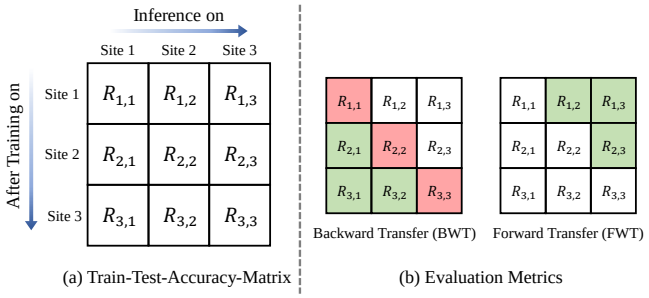

(a) Train-Test-Accuracy-Matrix (b) Evaluation Metrics

Fig. 3. Calculation of Backward Transfer (BWT) and Forward Transfer (FWT). (a) shows the creation of the Train-Test-Accuracy-Matrix, each $\boldsymbol{R_{i,j}}$ represents the reference score; (b) illustrates the calculation of FWT and BWT, FWT is calculated with the selected green cells while the BWT is calcualted by comparing the green and red cells.

excluded from the training process. The segmentation model is updated through the data stream while data samples from previous sites become unavailable upon the arrival of a new site. The segmentation performance is evaluated using Dice Similarity Coefficient (DSC) and Average Surface Distance (ASD), which are averaged across all labels.

We calculated two additional evaluation metrics, Backward Transfer (BWT) and Forward Transfer (FWT) based on DSC (as shwon in Fig. 3), to assess the model memorizability and generalizability during learning. We formulated the BWT and FWT following Ozgun *et al.* [38] as:

$$\begin{aligned} BWT &= \frac{2\sum_{i=2}^{n}\sum_{j=1}^{i-1} 1 - \left|\min\left(R_{i,j} - R_{j,j}, 0\right)\right|}{n(n-1)}, \\ FWT &= \frac{\sum_{i=1}^{n}\sum_{j=i+1}^{n} R_{i,j}}{\sum_{i=1}^{n-1}(n-i)}, \end{aligned} \tag{10}$$

where n is the number of sites and each $R_{i,j}$ represents the score of the model tested on site j after training on site i.

For better evaluating the backward transfer based on ASD, we replaced the BWT with BWT^+ as proposed in [39]:

$$BWT^{+} = \frac{2\sum_{i=2}^{n}\sum_{j=1}^{i-1} \max\left(R_{i,j} - R_{j,j}, 0\right)}{n(n-1)}. \tag{11}$$

B. Implementation Details

1) Network Architecture: We utilized a U-Net model configured with channel numbers 8, 16, 32, 64, and 128 for segmentation. We employed another U-Net as the diffusion model, with the first convolution layer consisting of 128 channels and an attention layer is integrated at the resolution of 16. Simulated images were generated with 1000 sampling steps. Learnable prompts are adaptable embeddings with dimension of 512, matching the time embedding dimension produced by the time encoder at each step of the diffusion process.

2) Training Configurations: The diffusion process was implemented on an NVIDIA GeForce RTX4090 GPU, we used Adam optimizer with learning rate 1×10^{-4} and 800,000 iterations. The segmentation process was trained on an NVIDIA Titan-V GPU using Adam optimizer with learning rate 5×10^{-4}. It is worth noting that, we assigned $\gamma = 5 \times 10^{-5}$ and $\beta = 5 \times 10^{-4}$ in Eq. (5).

C. Experiment Results on Two Segmentation Tasks

1) Preliminary Experiments and Analysis: To investigate whether and how the model suffers from forgetting issue and/or domain shift when it subsequently learns from the multi-source data, we initially set up two baseline models: (1) **JointTrain**, where the model is trained with the data of all sites. It is considered as the upper bound; (2) **FineTune**, where the model is continuously finetuned on a sequentially arrived data stream. Of note, we kept all training configurations and the network backbone of FineTune and JointTrain identical to the proposed SMG-Learning, ensuring the fairness.

As observed from the Baseline panel in the Table. I and Table. II, the performance of FineTune significantly drops compared to JointTrain on previous sites, especially on earlier seen sites, suggesting that the model tends to overfit on the data of the incoming site that leads to a loss of previously learnt knowledge. Additionally, both the JointTrain and Finetune model are struggle to maintain the satisfactory results on the unseen sites due to the domain shift across sites. These observations demonstrate that site-by-site finetuning leads to the catastrophic forgetting and has limited generalization ability.

2) Compared Methods: We compared our approach with several state-of-the-art methods under both Continual Learning (CL) and Domain Generalization (DG) frameworks. For CL-based methods, we explored (3) Elastic Weight Consolidation (**EWC**) [21] for implicitly and explicitly coordinated optimization; and (4) Continual-MAML (**C-MAML**) [40] for online-aware meta-learning optimization; (5) Generative Replay (**GR**) [39] addresses forgetting by constructing replay buffer from generative models. For DG-based algorithms, we implemented (6) **BigAug** [13], which proposes to combine multiple strong data augmentation strategies for better generalization; (7) **FISH** [14], which aligns inter-domain gradients for learning site-invariant features; and (8) Domain-oriented Feature Embedding (**DoFE**) [28] based on ensemble learning by utilizing knowledge from past sites.

3) Results on Prostate Image Segmentation: Experimental results of the prostate data are presented in Table. I. As observed, the CL-based methods achieve better results in the previous sites, while the DG-based approaches perform better on the unseen site. Such observations exactly conform to the inherent characteristics of these two approaches. The CL-based methods mainly focus on retaining previously learned knowledge to alleviate the forgetting, but struggle to generalize to unseen sites. For example, EWC and C-MAML adjust the model update direction, which potentially make model difficult to adapt to new sites nor generalize to unseen sites, with only around 86% DSC on incoming site E, and less than 89% DSC on unseen Site F. The replay-based GR method achieves 94.52% DSC on incoming site E but exhibits reduced accuracy on the previous sites, possibly due to artifacts in GAN-generated synthetic data. On the other hand, all DG methods achieve over 90% DSC on Site F, demonstrating their strong generalizability, yet score lower on previous sites, indicating a sacrifice in memorizability. On the contrary, Our method successfully optimizes the model towards synchronous memorizability and generalizability by employing SMG-Learning. It outperforms all compared methods by achieving a 2.13% improvement in overall DSC over the second-best method. Futhermore, our method achieves the highest BWT and FWT among all algorithms. We have visualized the prostate seg-

TABLE I

COMPARISON WITH THE STATE-OF-THE-ART APPROACHES ON PROSTATE IMAGE SEGMENTATION BY CONSECUTIVE LEARNING ON THE DATA STREAM FROM SITE A TO E. **BOLD** FONT REPRESENTS THE BEST RESULT (EXCEPT JOINTTRAIN PERFORMED OFFLINE).

		Previous				Incoming	Unseen	Overall	BWT	FWT	Previous				Incoming	Unseen	Overall	BWT+	FWT
		Site A	Site B	Site C	Site D	Site E	Site F				Site A	Site B	Site C	Site D	Site E	Site F			
		Dice Similarity Coefficient (DSC) (%) ↑									**Average Surface Distance (ASD) (mm) ↓**								
Baseline	JointTrain	94.10	93.27	91.62	89.14	95.04	92.92	92.68	99.23	78.43	0.47	0.48	1.00	0.82	0.43	0.91	0.69	0.01	1.63
	FineTune	68.58	85.69	60.39	73.07	93.22	84.62	77.60	86.36	65.83	18.12	10.26	28.80	20.10	1.35	11.84	15.08	7.97	4.09
CL-based	EWC [21]	**93.33**	85.98	88.73	92.49	86.28	88.72	89.26	95.19	66.97	1.35	0.96	4.26	**0.60**	1.65	0.81	1.60	2.27	3.06
	C-MAML [40]	87.56	83.10	76.99	87.54	86.34	88.84	85.06	94.52	74.72	0.77	1.25	4.19	0.74	1.17	2.77	1.82	0.73	2.76
	GR [39]	90.52	90.80	88.29	87.68	**94.52**	87.32	89.85	93.84	73.41	1.29	1.00	2.02	1.24	**0.52**	3.71	1.63	1.67	2.42
DG-based	FISH [14]	87.15	90.83	75.56	89.01	94.27	91.88	88.12	88.61	75.25	7.38	6.78	22.25	7.97	0.59	4.43	8.23	1.47	2.43
	DoFE [28]	90.45	90.12	87.91	83.29	90.97	90.86	88.93	95.50	75.48	1.12	0.72	3.42	1.05	1.04	0.89	1.37	1.29	2.23
	BigAug [13]	85.18	89.33	83.28	88.50	89.86	90.17	87.72	94.83	78.20	5.09	2.34	10.34	4.03	1.54	1.05	4.06	1.71	2.22
SMG-Learning	W/O Arbitrary	89.46	89.30	87.27	87.80	88.80	86.51	88.19	96.30	65.11	1.93	0.99	1.94	1.43	1.64	1.43	1.56	1.02	3.20
	W/O Orientational	88.39	89.93	85.55	89.15	87.76	91.69	88.75	96.15	66.56	1.32	0.81	1.78	1.05	1.66	0.77	1.23	0.74	3.19
	W/O SMD [20]	91.55	93.31	**89.73**	89.12	92.94	94.04	91.78	96.42	77.73	1.43	0.51	**1.31**	1.21	0.56	0.40	0.90	0.50	1.96
	SMG-Learning	92.22	**93.73**	88.80	**90.31**	92.56	**94.25**	**91.98**	**96.89**	**78.73**	**0.87**	**0.44**	1.68	1.03	0.67	**0.37**	**0.84**	**0.37**	**1.44**

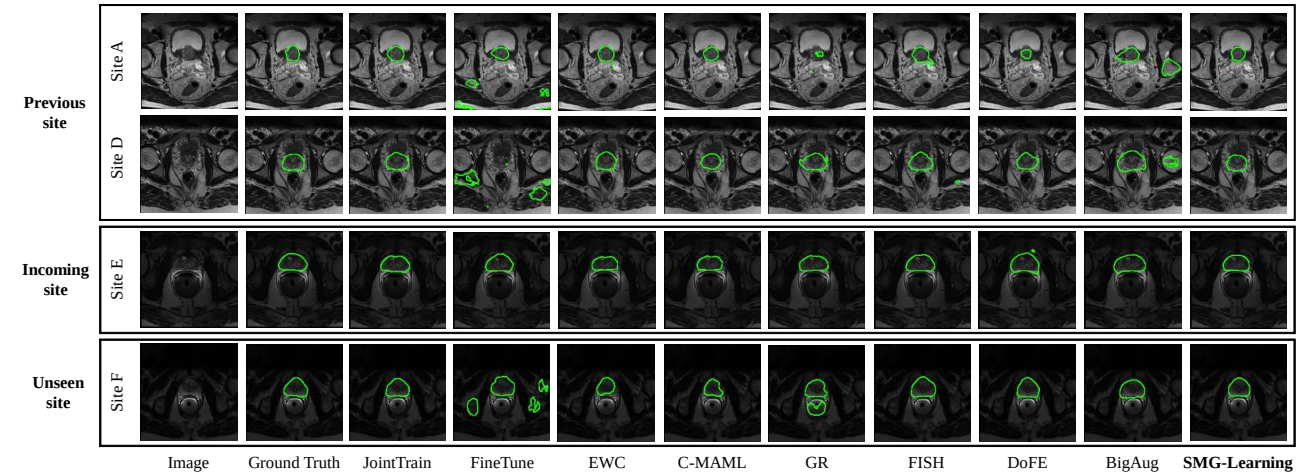

Fig. 4. Visual comparison for prostate image segmentation with data stream from site A to E, green contours indicating the predicted boundaries.

mentation results in Fig. 4, where our proposed SMG-Learning method closely approximates the ground truth and exhibits the highest overlap with JointTrain.

4) Results on Cardiac Image Segmentation: The quantitative comparison results in cardiac segmentation task are presented in Table. II. In this task, the issues of catastrophic forgetting and weak generalizability are less pronounced than in previous task, as indicated by the smaller performance gap between FineTune and JointTrain. Though other approaches effectively reduce forgetting and improve generalizability separately compared to FineTune, they fail to address both concurrently, resulting in lower overall DSC than JointTrain. Our propsed SMG-Learning method outperforms all other CL and DG methods, achieving the highest overall DSC that is 1.82% better than another CL-based generative method (GR), which demonstrates the superior of our generated replay images using site-modulated diffusion model over those generated by GAN-based model. Notably, our method nearly matches the performance of JointTrain, which serves as the upper bound, with only 0.58% lower overall DSC, indicating its exceptional ability to alleviate forgetting and optimize generalizability. Generally, CL-based methods obtain higher BWT, demonstrating their good memorability, while DG-based methods show higher FWT, indicating their satisfactory generalizability. Our method outperforms other approaches in both BWT and FWT, achieving the highest scores during consecutive learning. The segmentation results are visualized in Fig. 5, further demonstrate that our method performs the best.

D. Ablation Studies

1) Analysis of Each Module in SMG-Learning: We validated two complementary gradient alignments in our PGA method: 1) orientational gradient alignment, achieving coordinated optimization between incoming site and the replay buffer; 2) arbitrary gradient alignment, facilitating the invariance of extracted features among randomly split sub-sites. The results are shown in the last panel in Table I and II. 'W/O Arbitrary' implements only the orientational gradient alignment, which obtains improvement on previous sites but yields unsatisfied results on unseen site. Meanwhile, 'W/O Orientational' employs only arbitrary gradient alignment, enhancing performance on unseen site at the expense of reduced accuracy on previously sites. 'W/O SMD' represents the SMG-Learning without site-modulated diffusion model, obtaining higher overall DSC than other algorithms. Finally, our integrated SMG-Learning framework achieves synchronized optimization across all sites with the highest overall DSC score, demonstrating superior performance in both memorizability and generalizability.

TABLE II

COMPARISON WITH THE STATE-OF-THE-ART APPROACHES ON CARDIAC IMAGE SEGMENTATION BY CONSECUTIVE LEARNING ON THE DATA STREAM FROM VENDOR A TO C. **BOLD** FONT REPRESENTS THE BEST RESULT (EXCEPT JOINTTRAIN PERFORMED OFFLINE).

		Previous		Incoming	Unseen	Overall	BWT	FWT	Previous		Incoming	Unseen	Overall	BWT+	FWT
		Vendor A	Vendor B	Vendor C	Vendor D				Vendor A	Vendor B	Vendor C	Vendor D			
		Dice Similarity Coefficient (DSC) (%) ↑							Average Surface Distance (ASD) (mm) ↓						
Baseline	JointTrain	85.67	90.35	89.94	89.14	88.77	99.55	85.71	1.04	0.69	1.14	0.75	0.91	0	1.29
	FineTune	75.48	83.23	88.07	75.68	80.62	92.14	81.28	2.80	1.71	2.22	2.25	2.25	1.54	2.14
CL-based	EWC [21]	80.36	84.41	84.99	81.97	82.93	96.47	82.92	3.62	2.17	3.45	1.85	2.77	0.90	1.67
	C-MAML [40]	82.18	86.55	86.64	83.24	84.65	97.51	83.60	1.66	0.86	2.37	1.17	1.52	0.14	1.36
	GR [39]	83.76	86.93	87.85	86.95	86.37	96.80	83.77	1.84	2.44	2.22	2.61	2.28	0.06	1.69
DG-based	FISH [14]	82.78	88.16	89.13	86.29	86.59	95.96	83.67	1.26	0.76	1.59	0.78	1.10	0.47	1.51
	DoFE [28]	84.16	86.57	84.96	83.87	84.89	97.03	84.60	0.72	0.52	1.51	0.69	1.02	0.41	1.37
	BigAug [13]	85.01	88.33	84.29	87.59	86.30	97.54	83.58	0.79	0.88	3.71	**0.50**	1.47	0.49	1.61
SMG-Learning	W/O Arbitrary	81.01	84.16	89.26	78.90	83.33	96.36	83.41	1.11	0.74	0.84	1.00	0.92	0.33	1.67
	W/O Orientational	82.60	85.23	88.96	83.06	84.96	96.14	83.60	**0.68**	1.00	0.97	0.96	0.90	0.56	1.50
	W/O SMD [20]	85.11	**89.02**	88.93	**88.29**	87.83	97.53	83.72	0.89	0.82	1.20	1.08	1.00	0.12	1.48
	SMG-Learning	**85.99**	88.73	**90.10**	87.93	**88.19**	**99.35**	**85.08**	0.77	**0.57**	**0.79**	0.68	**0.70**	**0.03**	**1.14**

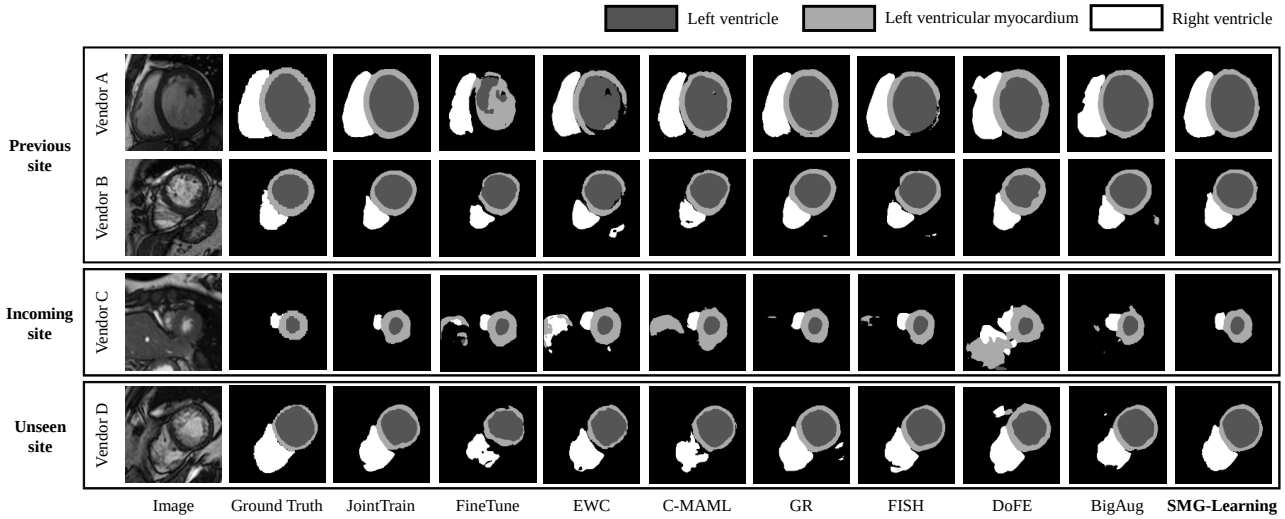

Fig. 5. Visual comparison for cardiac image segmentation with data stream from vendor A to C, with distinct colors representing different structures.

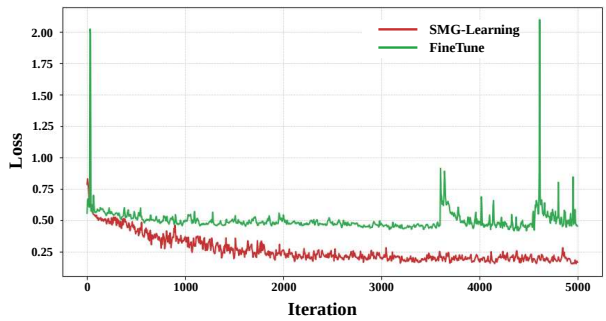

Fig. 6. The inference losses between FineTune and SMG-Learning on the combination of replay buffer and incoming site.

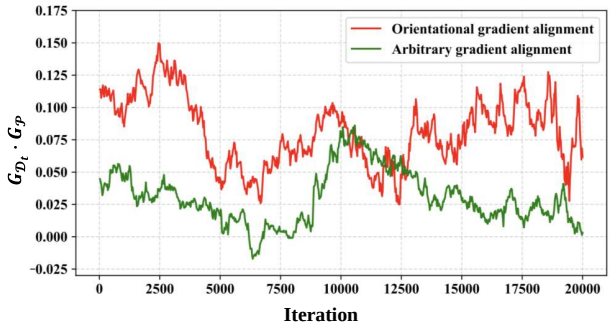

Fig. 7. The gradient inner product $G_{\mathcal{D}_t} \cdot G_{\mathcal{P}}$ when training on the combination of replay buffer and incoming site.

2) Analysis of Parallel Gradient Alignment: To evaluate the effectiveness of our PGA module, we trained both FineTune and SMG-Learning using incoming data and the replay buffer, and visualized their inference losses in Fig. 6. The loss for FineTune is higher and unstable due to unmatched optimization directions between the incoming site and past sites. Conversely, our method shows lower and smoother loss, indicating better convergence on the incoming site while maintaining good performance on previous and unseen sites.

We visualized the normalized inner product $G_{\mathcal{D}_t} \cdot G_{\mathcal{P}}$ in Fig. 7. Orientational gradient alignment particularly focuses on the $G_{\mathcal{D}_t} \cdot G_{\mathcal{P}}$, which results in a higher curve compared to arbitrary gradient alignment, indicating better memorability. Experiment result demonstrates that orientational gradient alignment ensures higher $G_{\mathcal{D}_t} \cdot G_{\mathcal{P}}$, thus maintaining it is crucial in the PGA objective despite it could be considered as a specialized case in the arbitrary gradient alignment.

3) Analysis under Different Training Sequences.: To demonstrate the robustness of our algorithm, we drew the error bar chart that records the overall DSC values for each model under three distinct training sequences in prostate segmentation task, as illustrated in Fig. 8. Sub-figure (a) represents sites arriving in alphabetical order (A→B→C→D→E), sub-figure (b) illustrates the reverse order (E→D→C→B→A), and

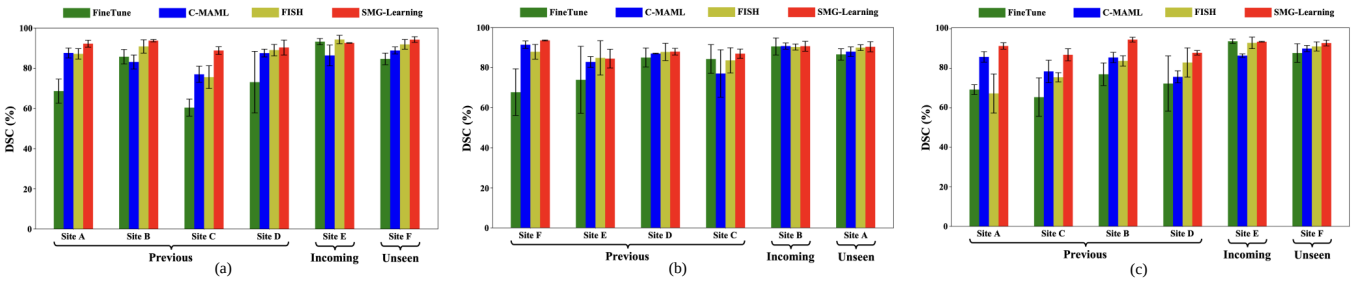

Fig. 8. Experiment results under three different training sequences: (a) normal sequence, (b) reverse sequence and (c) random sequence.

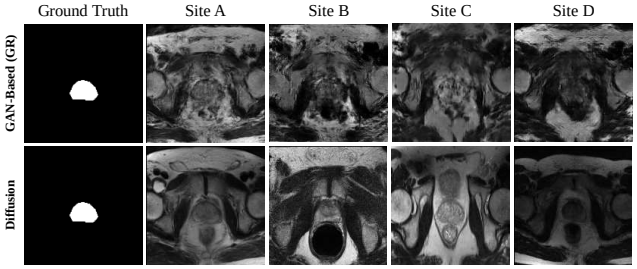

Fig. 9. Comparison between the generated replay images for past sites from site-modulated diffusion and GR with segmentation ground truth.

sub-figure (c) displays a random order (A→C→B→D→E). For evaluating the memorability and generalizability of each model, we conducted comparisons between our algorithm with FineTune, one CL-based method (C-MAML) and one DG-based method (FISH). As can be observed from this graph, our method (red bar) achieves the highest scores than other models across all distinct training sequences, which demonstrates the superiority and robustness of our SMG-Learning strategy.

4) Analysis of Site-Modulated Diffusion: We randomly picked some synthesis samples from the prostate segmentation task for analysing the generation quality between GAN-based Generative Replay (GR) method and the site-modulated diffusion model, as shown in Fig. 9. The sampling outcomes from the diffusion model contain fewer artifacts and clearer muscle context compared to those produced by the GR method. In addition, utilizing the site-specific learnable prompts enables the diffusion model to create site-specific replay images that simulate a variety of appearances aligned with diverse sites.

V. Discussion

Over the past few decades, advancements in deep learning have significantly improved medical image analysis, alleviating the workload of healthcare professionals and improving diagnostic precision. However, deploying models in real-world medical scenarios still presents many challenges like privacy constraints and data heterogeneity. Privacy restrictions hinder the data sharing across hospitals (even departments), leading to data scarcity that limits the suitability of a single model in various clinical data distributions. To address this issue, we propose an approach based on gradient alignment which enhances the model memorizablity and generalizability synchronously. Besides, in community health screenings, such as ophthalmic examinations, the variability in devices, collection angles, and lighting conditions leads to data heterogeneity (or domain shift), which influences the robustness of models. Our SMG-Learning algorithm overcomes these challenges through coordinated optimization, demonstrating essential clinical utility and resolves key challenges in real medical applications.

In the context of continual learning with a data stream, most existing approaches alleviate forgetting and improve stability by constructing a replay buffer, which preserves data from previous sites. However, given the concerns of privacy restriction and storage limitation, it is crucial to achieve a balanced trade-off between preservation capacity and model performance. Based on the efficacy requirement, we propose a diffusion model guided by learnable prompts for generating synthetic replay images. Our method only requires to store a trained diffusion model and site-specific learnable prompts (each less than 1MB). This strategy becomes increasingly efficient with the addition of more sites, since only the prompt require extra storage. Nonetheless, the drawback of our algorithm is the high time consumption finetuning diffusion model across various sites. Future work will focus on selectively optimizing parameters in the diffusion model that are sensitive to image style variations while keeping the rest fixed.

Recent studies have made significant achievements in employing foundation models for medical image analysis, mitigating performance degradation across diverse data distributions and tasks. The training paradigm for foundation models can be categorized into data-centric and model-centric approaches. On one hand, data-centric training paradigms require substantial annotated data. Our proposed generative method can generate numerous data-label pairs, which overcomes the challenge of medical data scarcity and reduces the manual labor costs of data annotation. On the other hand, model-centric approaches emphasise the design of the model structure. Our SMG-Learning strategy is adaptable to any model structure, it can be applied to any foundation model to enhance performance. Therefore, integrating our method with foundation model paradigms represents a promising direction.

VI. Conclusion

This work marks the first proposal of Synchronous Memorizability and Generalizability (SMG-Learning) for continual multi-site medical image segmentation. We propose a novel Parallel Gradient Alignments (PGA) approach with dual complementary gradient alignments to simultaneously mitigate forgetting and enhance generalizability. And we further optimize the computational complexity with dual meta-objectives. To address the data privacy constraints and storage limitation, we implement a Site-Modulated Diffusion (SMD) generative method to efficiently generate replay data. Experiments on prostate and cardiac segmentation tasks demonstrate the superiority of our method in achieving synchronous memorizability and generalizability over other SOTA CL and DG algorithms.

REFERENCES

[1] B. Kayalibay, G. Jensen, and P. van der Smagt, "Cnn-based segmentation of medical imaging data," *arXiv preprint arXiv:1701.03056*, 2017.

[2] Q. Liu, Q. Dou, L. Yu, and P. A. Heng, "Ms-net: multi-site network for improving prostate segmentation with heterogeneous mri data," *IEEE transactions on medical imaging*, vol. 39, no. 9, pp. 2713–2724, 2020.

[3] A. K. Upadhyay and A. K. Bhandari, "Advances in deep learning models for resolving medical image segmentation data scarcity problem: A topical review," *Archives of Computational Methods in Engineering*, pp. 1–19, 2023.

[4] L. Qu, N. Balachandar, M. Zhang, and D. Rubin, "Handling data heterogeneity with generative replay in collaborative learning for medical imaging," *Medical image analysis*, vol. 78, p. 102424, 2022.

[5] Z. Li, C. Zhong, R. Wang, and W.-S. Zheng, "Continual learning of new diseases with dual distillation and ensemble strategy," in *Medical Image Computing and Computer Assisted Intervention–MICCAI 2020: 23rd International Conference, Lima, Peru, October 4–8, 2020, Proceedings, Part I 23*. Springer, 2020, pp. 169–178.

[6] Q. Liu, C. Chen, J. Qin, Q. Dou, and P.-A. Heng, "Feddg: Federated domain generalization on medical image segmentation via episodic learning in continuous frequency space," in *Proceedings of the IEEE/CVF Conference on Computer Vision and Pattern Recognition*, 2021, pp. 1013–1023.

[7] P. W. Koh, S. Sagawa, H. Marklund, S. M. Xie, M. Zhang, A. Balsubramani, W. Hu, M. Yasunaga, R. L. Phillips, I. Gao *et al.*, "Wilds: A benchmark of in-the-wild distribution shifts," in *International conference on machine learning*. PMLR, 2021, pp. 5637–5664.

[8] L. Wang, X. Zhang, H. Su, and J. Zhu, "A comprehensive survey of continual learning: Theory, method and application," *IEEE Transactions on Pattern Analysis and Machine Intelligence*, 2024.

[9] A. Chaudhry, P. K. Dokania, T. Ajanthan, and P. H. Torr, "Riemannian walk for incremental learning: Understanding forgetting and intransigence," in *Proceedings of the European conference on computer vision (ECCV)*, 2018, pp. 532–547.

[10] R. Aljundi, F. Babiloni, M. Elhoseiny, M. Rohrbach, and T. Tuytelaars, "Memory aware synapses: Learning what (not) to forget," in *Proceedings of the European conference on computer vision (ECCV)*, 2018, pp. 139–154.

[11] M. Perkonigg, J. Hofmanninger, and G. Langs, "Continual active learning for efficient adaptation of machine learning models to changing image acquisition," in *International Conference on Information Processing in Medical Imaging*. Springer, 2021, pp. 649–660.

[12] Y. Ganin, E. Ustinova, H. Ajakan, P. Germain, H. Larochelle, F. Laviolette, M. March, and V. Lempitsky, "Domain-adversarial training of neural networks," *Journal of machine learning research*, vol. 17, no. 59, pp. 1–35, 2016.

[13] L. Zhang, X. Wang, D. Yang, T. Sanford, S. Harmon, B. Turkbey, B. J. Wood, H. Roth, A. Myronenko, D. Xu *et al.*, "Generalizing deep learning for medical image segmentation to unseen domains via deep stacked transformation," *IEEE transactions on medical imaging*, vol. 39, no. 7, pp. 2531–2540, 2020.

[14] Y. Shi, J. Seely, P. H. Torr, N. Siddharth, A. Hannun, N. Usunier, and G. Synnaeve, "Gradient matching for domain generalization," *arXiv preprint arXiv:2104.09937*, 2021.

[15] S. Zhao, M. Gong, T. Liu, H. Fu, and D. Tao, "Domain generalization via entropy regularization," *Advances in neural information processing systems*, vol. 33, pp. 16 096–16 107, 2020.

[16] M. Riemer, I. Cases, R. Ajemian, M. Liu, I. Rish, Y. Tu, and G. Tesauro, "Learning to learn without forgetting by maximizing transfer and minimizing interference," *arXiv preprint arXiv:1810.11910*, 2018.

[17] J. Yoon, W. Jeong, G. Lee, E. Yang, and S. J. Hwang, "Federated continual learning with weighted inter-client transfer," in *International Conference on Machine Learning*. PMLR, 2021, pp. 12 073–12 086.

[18] S. Du, X. Wang, Y. Lu, Y. Zhou, S. Zhang, A. Yuille, K. Li, and Z. Zhou, "Boosting dermatoscopic lesion segmentation via diffusion models with visual and textual prompts," *arXiv preprint arXiv:2310.02906*, 2023.

[19] L. Zhang, A. Rao, and M. Agrawala, "Adding conditional control to text-to-image diffusion models," in *Proceedings of the IEEE/CVF International Conference on Computer Vision*, 2023, pp. 3836–3847.

[20] J. Zhang, P. Xue, R. Gu, Y. Gu, M. Liu, Y. Pan, Z. Cui, J. Huang, L. Ma, and D. Shen, "Learning towards synchronous network memorizability and generalizability for continual segmentation across multiple sites," in *International Conference on Medical Image Computing and Computer-Assisted Intervention*. Springer, 2022, pp. 380–390.

[21] J. Kirkpatrick, R. Pascanu, N. Rabinowitz, J. Veness, G. Desjardins, A. A. Rusu, K. Milan, J. Quan, T. Ramalho, A. Grabska-Barwinska *et al.*, "Overcoming catastrophic forgetting in neural networks," *Proceedings of the national academy of sciences*, vol. 114, no. 13, pp. 3521–3526, 2017.

[22] V. Marsocci and S. Scardapane, "Continual barlow twins: continual self-supervised learning for remote sensing semantic segmentation," *IEEE Journal of Selected Topics in Applied Earth Observations and Remote Sensing*, 2023.

[23] Q. Sun, F. Lyu, F. Shang, W. Feng, and L. Wan, "Exploring example influence in continual learning," *Advances in Neural Information Processing Systems*, vol. 35, pp. 27 075–27 086, 2022.

[24] H. Jin and E. Kim, "Helpful or harmful: Inter-task association in continual learning," in *European Conference on Computer Vision*. Springer, 2022, pp. 519–535.

[25] Z. Wang, M. Loog, and J. Van Gemert, "Respecting domain relations: Hypothesis invariance for domain generalization," in *2020 25th International Conference on Pattern Recognition (ICPR)*. IEEE, 2021, pp. 9756–9763.

[26] D. Li, Y. Yang, Y.-Z. Song, and T. Hospedales, "Learning to generalize: Meta-learning for domain generalization," in *Proceedings of the AAAI conference on artificial intelligence*, vol. 32, no. 1, 2018.

[27] C. Finn, P. Abbeel, and S. Levine, "Model-agnostic meta-learning for fast adaptation of deep networks," in *International conference on machine learning*. PMLR, 2017, pp. 1126–1135.

[28] S. Wang, L. Yu, K. Li, X. Yang, C.-W. Fu, and P.-A. Heng, "Dofe: Domain-oriented feature embedding for generalizable fundus image segmentation on unseen datasets," *IEEE Transactions on Medical Imaging*, vol. 39, no. 12, pp. 4237–4248, 2020.

[29] M. Zhai, L. Chen, F. Tung, J. He, M. Nawhal, and G. Mori, "Lifelong gan: Continual learning for conditional image generation," in *Proceedings of the IEEE/CVF international conference on computer vision*, 2019, pp. 2759–2768.

[30] K. Binici, S. Aggarwal, N. T. Pham, K. Leman, and T. Mitra, "Robust and resource-efficient data-free knowledge distillation by generative pseudo replay," in *Proceedings of the AAAI Conference on Artificial Intelligence*, vol. 36, no. 6, 2022, pp. 6089–6096.

[31] R. Gao and W. Liu, "Ddgr: Continual learning with deep diffusion-based generative replay," in *International Conference on Machine Learning*. PMLR, 2023, pp. 10 744–10 763.

[32] D. Lopez-Paz and M. Ranzato, "Gradient episodic memory for continual learning," *Advances in neural information processing systems*, vol. 30, 2017.

[33] Q. Liu, Q. Dou, and P.-A. Heng, "Shape-aware meta-learning for generalizing prostate mri segmentation to unseen domains," in *Medical Image Computing and Computer Assisted Intervention–MICCAI 2020: 23rd International Conference, Lima, Peru, October 4–8, 2020, Proceedings, Part II 23*. Springer, 2020, pp. 475–485.

[34] N. Bloch, A. Madabhushi, H. Huisman, J. Freymann, J. Kirby, M. Grauer, A. Enquobahrie, C. Jaffe, L. Clarke, and K. Farahani, "Nci-isbi 2013 challenge: Automated segmentation of prostate structures," The Cancer Imaging Archive, 2015.

[35] G. Lemaître, R. Martí, J. Freixenet, J. C. Vilanova, P. M. Walker, and F. Meriaudeau, "Computer-aided detection and diagnosis for prostate cancer based on mono and multi-parametric mri: a review," *Computers in biology and medicine*, vol. 60, pp. 8–31, 2015.

[36] G. Litjens, R. Toth, W. Van De Ven, C. Hoeks, S. Kerkstra, B. Van Ginneken, G. Vincent, G. Guillard, N. Birbeck, J. Zhang *et al.*, "Evaluation of prostate segmentation algorithms for mri: the promise12 challenge," *Medical image analysis*, vol. 18, no. 2, pp. 359–373, 2014.

[37] V. M. Campello, P. Gkontra, C. Izquierdo, C. Martin-Isla, A. Sojoudi, P. M. Full, K. Maier-Hein, Y. Zhang, Z. He, J. Ma *et al.*, "Multi-centre, multi-vendor and multi-disease cardiac segmentation: the m&ms challenge," *IEEE Transactions on Medical Imaging*, vol. 40, no. 12, pp. 3543–3554, 2021.

[38] S. Özgün, A.-M. Rickmann, A. G. Roy, and C. Wachinger, "Importance driven continual learning for segmentation across domains," in *Machine Learning in Medical Imaging: 11th International Workshop, MLMI 2020, Held in Conjunction with MICCAI 2020, Lima, Peru, October 4, 2020, Proceedings 11*. Springer, 2020, pp. 423–433.

[39] K. Li, L. Yu, and P.-A. Heng, "Domain-incremental cardiac image segmentation with style-oriented replay and domain-sensitive feature whitening," *IEEE Transactions on Medical Imaging*, vol. 42, no. 3, pp. 570–581, 2022.

[40] G. Gupta, K. Yadav, and L. Paull, "Look-ahead meta learning for continual learning," *Advances in Neural Information Processing Systems*, vol. 33, pp. 11 588–11 598, 2020.